
SAMPLE EFFICIENT ROBOT LEARNING IN SUPERVISED EFFECT PREDICTION TASKS

A PREPRINT

✉ Mehmet Arda Eren^{*1} and ✉ Erhan Oztop^{†1,2}

¹Department of Artificial Intelligence, Ozyegin University, Istanbul, Turkey

²OTRI/SISReC, Osaka University, Osaka, Japan

ABSTRACT

In self-supervised robot learning, robots actively explore their environments and generate data by acting on entities in the environment. Therefore, an exploration policy is desired that ensures sample efficiency to minimize robot execution costs while still providing accurate learning. For this purpose, the robotic community has adopted Intrinsic Motivation (IM)-based approaches such as Learning Progress (LP). On the machine learning front, Active Learning (AL) has been used successfully, especially for classification tasks. In this work, we develop a novel AL framework geared towards robotics regression tasks, such as action-effect prediction and, more generally, for world model learning, which we call MUSEL - Model Uncertainty for Sample Efficient Learning. MUSEL aims to extract model uncertainty from the total uncertainty estimate given by a suitable learning engine by making use of earning progress and input diversity and use it to improve sample efficiency beyond the state-of-the-art action-effect prediction methods. We demonstrate the feasibility of our model by using a Stochastic Variational Gaussian Process (SVGP) as the learning engine and testing the system on a set of robotic experiments in simulation. The efficacy of MUSEL is demonstrated by comparing its performance to standard methods used in robot action-effect learning. In a robotic tabletop environment in which a robot manipulator is tasked with learning the effect of its actions, the experiments show that MUSEL facilitates higher accuracy in learning action effects while ensuring sample efficiency.

Keywords Robot Active Learning · Sample Efficiency · Effect Prediction · Uncertainty Estimation

1 Introduction

A fundamental challenge in enabling robots to operate efficiently in complex environments is developing their ability to plan and execute actions effectively. One promising way to equip robots with planning capability is to let them learn the effect of their actions in a self-supervised manner [Ahmetoglu et al., 2022, Seker et al., 2019, Ugur et al., 2011]. In simulation, this can be carried out by generating random action parameters for a range of environment configurations in which the robot executes the actions and records the observed effect. This is akin to building a simplified world model [Ha and Schmidhuber, 2018]. Although this works, it is not ideal as action selection is not guided towards maximizing sample efficiency, and thus it is not usually feasible for real robot learning where execution is costly.

Sample efficiency in robot learning is often considered in conjunction with reinforcement learning (RL) [Baranes and Oudeyer, 2013, Li et al., 2023], and explicit addressing of sample efficiency in self-supervised learning is limited [Oudeyer et al., 2007, Péré et al., 2018, Sener et al., 2021, Bugur et al., 2019], which we aim to contribute with this work. For supervised learning tasks, Intrinsic Motivation (IM) and Active Learning (AL) stands as two candidates. Intrinsic motivation involves the robot's internal drive to explore and learn based on its own progress or discoveries, prompting it to seek new experiences or challenges without being directed by external objectives. However, IM is not

*arda.eren@ozu.edu.tr

†erhan.oztop@otri.osaka-u.ac.jp

specifically designed to optimize sample efficiency. On the other hand, Active learning algorithms selectively query the most informative data points, aiming to improve learning efficiency by reducing the amount of labeled data needed.

In AL-based approaches, data selection for learning can be guided by three measurements [Settles, 2009, He et al., 2014]: informativeness [Käding et al., 2018, Cai et al., 2013, Sugiyama and Nakajima, 2009, Wu, 2018, Liu et al., 2021], representativeness [Wu, 2018], and diversity [Wu et al., 2019, Wu, 2018, Liu et al., 2021]. These techniques are not directly applicable to robot self-learning tasks, as most AL techniques require a finite data space or an approximation for the continuous set of state-action pairs [Taylor et al., 2021] and spatial solutions to find a finite representation or approximation are computationally expensive [van Deursen, 2020].

In this study, we propose a novel active learning algorithm called Model Uncertainty for Sample-Efficient Learning (MUSEL) for sample-efficient robot self-supervised learning. MUSEL is designed for supervised robot prediction tasks with continuous input spaces and multi-dimensional output. It uses a Stochastic Variational Gaussian Process (SVGP) [Hensman et al., 2013] to estimate combined data and model uncertainty associated with a prediction task, and extracts model uncertainty by using Learning Progress (LP) [Kaplan and Oudeyer, 2004, Oudeyer et al., 2007] and Input Greedy Sampling [Wu et al., 2019]. To demonstrate the applicability of our method to self-supervised effect prediction tasks, a simulated robotic environment is used where a 7-degrees-of-freedom (DOF) robot interacts with its environment. Experiments are conducted to assess the sample efficiency of the method. Ablation studies are also performed to provide insight into the components of the model. The main contributions of this study can be given in the following.

- Extraction of model uncertainty from total uncertainty using learning progress and input diversity.
- Use of model uncertainty-based sample selection in robot action effect prediction learning.
- Development of a concrete active learning algorithm for action-effect prediction applicable to continuous action and state settings.
- Demonstration of the applicability of our method to nontrivial robot self-supervised learning tasks.

In the remainder of the paper, the scientific background and related work is given in the next section. The details of the methods used in the study are detailed in Methods. The experiments and related results are presented in the Experiments and Results section. Finally, Conclusion concludes the paper.

2 Related Work

2.1 Active Learning and Its Application in Robotics

Active Learning (AL) [Cohn et al., 1996], defined by strategic selection of the training data, enhances model performance while reducing costs, thus finding applications across a wide range of fields. AL algorithms primarily address supervised tasks with specialized selection strategies developed for both classification [Liu et al., 2021, Fu et al., 2013] and regression tasks [Käding et al., 2018, Wu, 2018, Wu et al., 2019, Cai et al., 2013]. Furthermore, these methods can be divided into two categories based on the presence of an iteration inside the algorithm: supervised [Fu et al., 2013, Käding et al., 2018, Wu, 2018, Wu et al., 2019, Cai et al., 2013] and unsupervised [Liu et al., 2021]. Another classification of AL methods can be made based on the used sampling set. When the set is finite, the methods are often called pool-based; whereas, when the sampling set is infinite, they are known as population-based [Sugiyama and Nakajima, 2009]. To address the continuous input-output structure generally observed in robotic tasks, MUSEL is designed as a supervised and population-based AL framework that specifically targets regression tasks.

Motivated by its success in other applications, AL has been utilized across various domains in robotics, as discussed in [Taylor et al., 2021], including environmental mapping [Lluvia et al., 2021], non-parametric shape estimation [Abraham et al., 2017], robot control [Andersson et al., 2017, Maeda et al., 2017], perception and prediction [Segal et al., 2022], and distributed learning [Jang et al., 2021]. However, these approaches typically treat exploration and efficiency as separate objectives. In our work, we address this issue by utilizing uncertainty-based sampling to balance both, enabling sample-efficient supervised effect prediction in robotic tasks.

Notably, Intrinsic Motivation (IM) can also be used to efficiently gather training samples by selecting actions based on an internal motivational signal related to novelty or surprise [Oudeyer et al., 2007]. Metrics commonly used for IM include error maximization [Marshall et al., 2004, Huang and Weng, 2002], information maximization [Houthoofd et al., 2016], surprise factor [Achiam and Sastry, 2017], and learning progress (LP) [Oudeyer et al., 2007, Bugur et al., 2019, Say and Oztop, 2023]. Furthermore, numerous studies in the literature employ IM approaches inspired by AL methods [Oudeyer et al., 2007, Baranes and Oudeyer, 2009]. Among the approaches mentioned above, inspired its applications

in robotic environments [Bugur et al., 2019, Say and Oztop, 2023], LP strategy contributes to our sample selection criteria by estimating data uncertainty (Section 3.4) and is directly compared with MUSEL in the results section.

Alternatively, the problem we address can also be explained from the neuroscience perspective. The term Active Sensing [Yang et al., 2016] refers to the manipulation of the state of a living being to gather more informative data about a given task. Here, the goal is to seek the actions that leads to most informative observations. In this sense, since the robot adjusts system parameters to reduce environmental uncertainty (Algorithm 1, line 14), MUSCLE can be described as an Active Sensing framework. There are also works in this area focused on sample-efficient learning, but they differ in objectives and methods, incorporating task-relevancy metrics [Greigarn et al., 2019, Tschantz et al., 2020] or emphasizing trajectory optimization [Chen et al., 2021, Napolitano et al., 2024], whereas our approach utilizes model uncertainty for efficient sample selection in continuous spaces.

2.2 Uncertainty Quantification

Uncertainty is a commonly used measure in AL algorithms for making sampling decisions [Yang and Loog, 2016, Yang et al., 2015, Zhu et al., 2009]. For this, usually the learning system is designed so as to generate both the prediction and its uncertainty as the output [Gawlikowski et al., 2021]. Various learning models have been developed for classification tasks [Sensoy et al., 2018, Oberdiek et al., 2018, Dias and Vermunt, 2006, Mena et al., 2021] as well as regression [Gawlikowski et al., 2021, Tripathy et al., 2016, Amini et al., 2020, Meinert and Lavin, 2021, Meinert et al., 2023].

Gaussian Process Regression (GPR) is popular model used for regression tasks, where the model generates the parameters of Normal distribution as output [Williams and Rasmussen, 1995]. The mean of the distribution serves as the prediction, while the standard deviation serves as the uncertainty associated with the prediction. Nonetheless, these models are not scalable by the large datasets, caused by the growth of the time and memory complexity by increase of the data [Tripathy et al., 2016].

Stochastic Variational Gaussian Processes (SVGP) [Titsias, 2009, Hensman et al., 2013, Gal et al., 2014], which we make use of in the study, use sparse approximations and variational inference to address the computational limits of traditional Gaussian Processes. By introducing inducing points, SVGP reduces complexity to linear in the data and cubic in the inducing points, while variational inference optimizes an Evidence Lower Bound (ELBO) [Blei et al., 2017] for scalability in large datasets.

3 Method

3.1 Problem Domain Formalization

We envision a robot that is tasked with learning the effects of its actions by interacting with the environment by collecting experiences of the form $(state, action) \rightarrow effect$, where *state* describes robot and environment configuration. Robot actions are costly, so the robot must learn an accurate model by minimizing the number of interactions with the environment. Towards this goal, the robot is equipped with an uncertainty estimation mechanism that guides its action selection, which is explained in the following sections. For clarity, we describe the proposed method linked to the robot task environment used for evaluating the model; but the approach is general and can be applied to any effect prediction task. Noting that this is a supervised learning problem, the set of inputs corresponding to a set of robot experiences can be given as $\mathbb{X} = \{x^t | x^t = (s^t, a^t), \text{ with } s^t \in S \subset \mathbb{R}^m, a^t \in A \subset \mathbb{R}^n\}$, where S and A are the state and actions spaces with the dimensions m, n corresponding to the robot task at hand, and t is an arbitrary sample index or time. In the experiments conducted in this study, s^t is a vector containing the 2D coordinate of a sphere to be interacted with (Exp. 1) or the concatenation of the two-sphere coordinates (Exp. 2), where the robot interacts with one of them and the other sphere act as a dynamic entity in the environment. The action, a^t , is defined as a real scalar indicating the hit angle of the robot. In the experiments, we assume that the robot can request the sphere(s) to be placed anywhere within the defined workspace, and decide its hit angle. The effects are the new location(s) of the sphere(s) after the robot action execution. Referring to (s^t, a^t) compactly as input x^t , the effect set associated with a set of inputs is then given by $\mathbb{Y} = \{y^t | y^t \in \mathbb{R}^r \text{ effect obtained with input } x^t \in \mathbb{X}\}$, where r is the effect space dimension.

3.2 Proposed Method: MUSEL

In this section, we explain our proposed model, MUSEL, which aims to minimize the number of observation queries while learning an input-output mapping over continuous spaces without sacrificing prediction accuracy. Specifically, in the robotic domain, we seek to enable a robot to learn the effects of its actions with as few executions as possible. At the core of MUSEL is the model uncertainty estimation method introduced in Section 3.4, which is embedded in a loop comprising *execution sample selection*, *robot execution*, *model learning*, and *input sampling*, as illustrated in Figure 1.

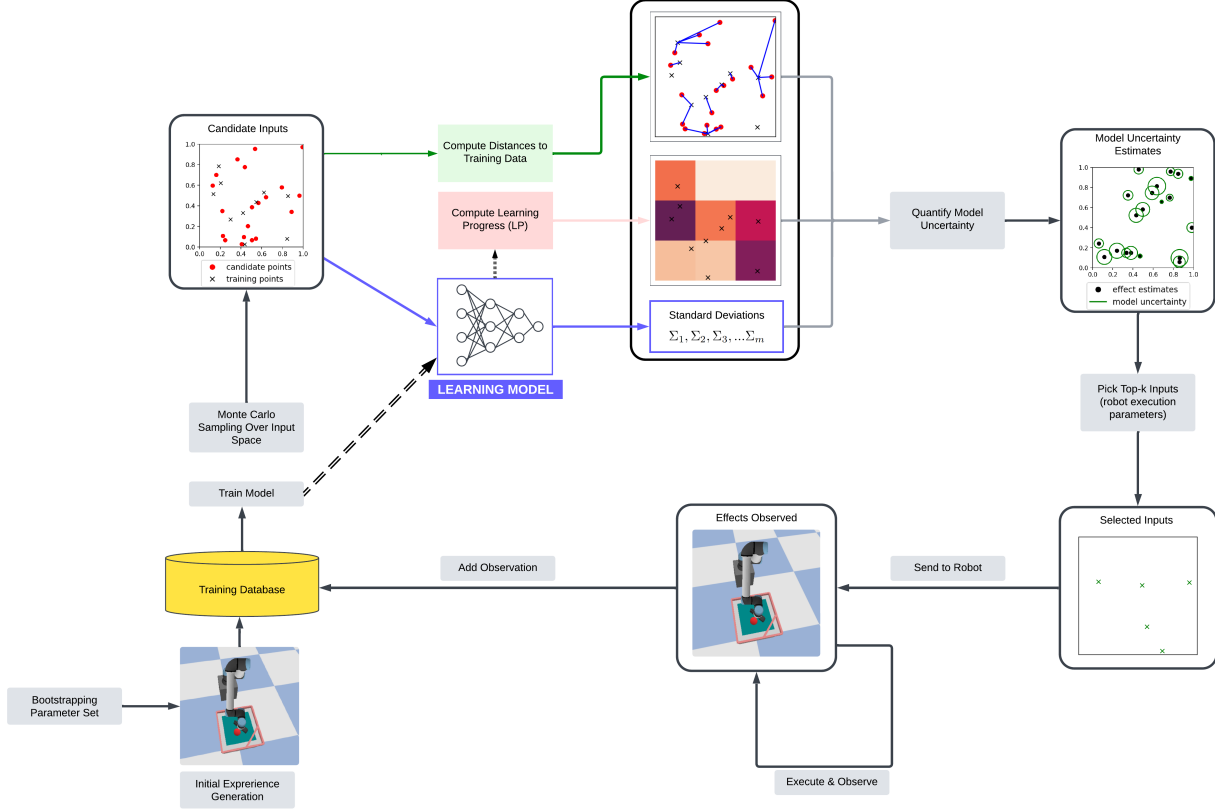


Figure 1: Illustration of the MUSEL framework

Learning with MUSEL begins with the initialization of the training data set to bootstrap model learning, which can contain as little as a single sample. Using this dataset, the weights of the learning model are updated, and the standard deviations and the error metrics required to compute Learning Progress (LP) are collected. Then, a set of m independently and identically distributed (i.i.d.) random inputs (state-action pairs) is generated from the input range. For each input in this set, the shortest distance to the samples used so far is calculated (Equation 11). The standard deviations, LP values, and shortest distances are then combined to quantify model uncertainties (Equation 12). Based on these estimates, the top k inputs (state-action pairs) are selected for the robot to execute, generating observations that are then incorporated into the training dataset (Algorithm 1, lines 15-16). This iterative process continues with model retraining and candidate generation until a specified iteration limit is reached.

In the following sections, we first provide a detailed explanation of the SVGP model, which serves as the learning engine of the MUSEL framework and is capable of producing prediction uncertainties alongside predictions. Next, we present our approach for *model uncertainty quantification*, followed by a detailed algorithm specification for implementing the MUSEL framework.

3.3 Stochastic Variational Gaussian Processes

The Stochastic Variational Gaussian Process (SVGP) is a probabilistic model that approximates the traditional Gaussian Processes (GPs) to efficiently generate uncertainty estimates without being constrained by scalability issues. We adopt SVGP as the backbone model of the MUSEL approach due to its ability to provide accurate uncertainty estimates while efficiently handling large datasets. In this section, first, we explain the working mechanism of traditional GPs, followed by a demonstration of the transition to SVGPs.

Instead of approximating a function, GP considers an infinite collection of possible functions that could explain the data. It does this by defining a probability distribution over these functions, allowing us to make predictions with associated uncertainty as shown in Equation 1. \mathbf{m} is the mean vector, \mathbf{K} is the covariance matrix, computed using a kernel function $k(\mathbf{x}_i, \mathbf{x}_j)$, and σ^2 is the noise variance.

$$f(\mathbf{X}) \sim \mathcal{N}(\mathbf{m}, \mathbf{K} + \sigma^2 \mathbf{I}) \quad (1)$$

The aim of GPs is to approximate y values by optimizing their kernel function parameters. To do that, the likelihood of observing the outputs y given the inputs X and parameters Θ , as shown in Equation 2, is used to find the optimal parameters.

$$p(\mathbf{y}|\mathbf{X}, \theta) = \int p(\mathbf{y}|f, \mathbf{X})p(f|\mathbf{X}, \theta) df \quad (2)$$

However, traditional GPs suffer from $O(N^3)$ computational complexity and $O(N^2)$ memory requirements that limits their usage with large datasets. This is because the log-marginal-likelihood, shown in Equation 3, requires an inverse of the \mathbf{K} value, which can be done in $O(N^3)$ time, which explained in Rasmussen and Williams [2006].

$$\log p(\mathbf{y}|\mathbf{X}, \theta) = -\frac{1}{2} \mathbf{y}^\top (\mathbf{K} + \sigma^2 \mathbf{I})^{-1} \mathbf{y} - \frac{1}{2} \log |\mathbf{K} + \sigma^2 \mathbf{I}| - \frac{n}{2} \log 2\pi \quad (3)$$

SVGP [Hensman et al., 2013] addresses this issue by defining a set of M inducing points \mathbf{Z} where $M \ll N$, and corresponding inducing variables $\mathbf{u} = f(\mathbf{Z})$. Also a variational distribution $q(\mathbf{u})$, a Gaussian distribution parameterized by \mathbf{m} and \mathbf{S} , is defined over the inducing variables:

$$q(\mathbf{u}) = \mathcal{N}(\mathbf{u}; \mathbf{m}, \mathbf{S}) \quad (4)$$

This way, the probability $p(\mathbf{y}|\mathbf{X}, \theta)$ is approximated using the inducing points, as shown in Equation 5. However, calculation using the equation is intractable since it contains nested integrals over f and u values, as explained in Titsias [2009].

$$p(\mathbf{y}|\mathbf{X}, \theta) \approx \int p(\mathbf{y}|\mathbf{f}, \mathbf{X})p(\mathbf{f}|\mathbf{u}, \mathbf{X})q(\mathbf{u}) d\mathbf{f} d\mathbf{u} \quad (5)$$

To overcome this issue, instead of trying to maximize the likelihood directly, the Evidence Lower Bound (ELBO) [Blei et al., 2017] is maximized instead. The ELBO, shown in Equation 6, calculates how the inducing points represent the data and how well the variational distribution fits the inducing points. Since evaluating the ELBO directly over large datasets is computationally infeasible, SVGP utilizes mini-batch stochastic gradient descent to optimize the ELBO where B is the mini-batch size, as shown in Hensman et al. [2013].

$$\text{ELBO} \approx \sum_{i=1}^B \mathbb{E}_{q(\mathbf{u})} [\log p(y_i|\mathbf{u})] - \text{KL}(q(\mathbf{u})||p(\mathbf{u})) \quad (6)$$

As stated in Blei et al. [2017], the equation consists of two parts: Expected Log Likelihood (Equation 7) and the KL-divergence (Equation 8). The Expected Log Likelihood term measures how well the variational distribution $q(\mathbf{u})$ explains the observed data \mathbf{y} . It involves computing the expectation of the log-likelihood of the data given the inducing variables:

$$\mathbb{E}_{q(\mathbf{u})} [\log p(\mathbf{y}|\mathbf{u})] = -\frac{1}{2\sigma^2} (\mathbf{y}^\top (\mathbf{K}_{\mathbf{X}\mathbf{X}} + \sigma^2 \mathbf{I})^{-1} \mathbf{y}) - \frac{N}{2} \log 2\pi\sigma^2 \quad (7)$$

The KL divergence term, as explained in Gal et al. [2014], regularizes the variational distribution $q(\mathbf{u})$ to prevent diverging from the prior distribution $p(\mathbf{u})$. It is defined as:

$$\text{KL}(q(\mathbf{u})||p(\mathbf{u})) = \frac{1}{2} \left(\text{tr}(\mathbf{K}_{\mathbf{Z}\mathbf{Z}}^{-1} \mathbf{S}) + \mathbf{m}^\top \mathbf{K}_{\mathbf{Z}\mathbf{Z}}^{-1} \mathbf{m} - M + \log \frac{|\mathbf{K}_{\mathbf{Z}\mathbf{Z}}|}{|\mathbf{S}|} \right) \quad (8)$$

In the ELBO [Hensman et al., 2013], the $\mathbf{K}_{\mathbf{X}\mathbf{X}}$ value is defined as $\mathbf{K}_{\mathbf{X}\mathbf{X}} \approx \mathbf{K}_{\mathbf{X}\mathbf{Z}} \mathbf{K}_{\mathbf{Z}\mathbf{Z}}^{-1} \mathbf{K}_{\mathbf{Z}\mathbf{X}}$. So the time complexity required for the taking inverse of the kernel is reduced from $O(N^3)$ to $O(NM^2)$. Also, the memory complexity is reduced from $O(N^2)$ to $O(M^2)$. Therefore it is much more suitable to use SVGPs in our task because the iterative characteristic of our AL algorithm requires fast training speeds.

Overall, the SVGP model is capable of producing the same variables as GPs, namely $\{\mu, \sigma\}$ as the predicted mean and standard deviation associated with a given input, without having the scalability problems of traditional GPs. In the next section, we take σ as the total uncertainty and combine it with other measures to drive a model uncertainty estimate.

3.4 Estimating Model Uncertainty

The total uncertainty associated with a prediction is a compound of data and model uncertainties [Gawlikowski et al., 2021]. We take the standard deviation output of SVGP on input x , $\sigma(x)$ as the total uncertainty associated with it and show it by $U(x)$. As a learner can only reduce the model uncertainty, we wish to estimate model uncertainty and then guide sample selection by it. To do this, following Lee et al. [2024], we assume statistical independence between the model uncertainty, U_{model} and data uncertainty, U_{data} and write

$$U(x) = \sigma(x) = U_{model}(x)U_{data}(x) \quad (9)$$

Since we have $\sigma(x)$ from SVGP, if we can estimate data uncertainty, $U_{data}(x)$, we will have an estimate on $U_{model}(x)$. As LP measures the rate of decrease in learning loss, a near zero or low LP indicates that the model performance does not increase and learning has saturated. This suggests the presence of data uncertainty; thus we can establish an inverse relationship between LP and data uncertainty. In addition, if there is high total uncertainty in a region where dense training data is present, we may conclude that the uncertainty there is due to data uncertainty as many points there were ineffective in reducing the error. To capture this logic, we introduce $\ell(x)$ that measures the distance from the data samples used in the training and propose the following data uncertainty estimate:

$$U_{data}(x) = \frac{1}{\ell(x)LP(x)} \quad (10)$$

where $\ell(x)$ is the minimum-distance (MD) to the training inputs, given as

$$\ell(x) = \min\{\|x - x_k\| \mid x_k \in O\} \quad (11)$$

with O representing the set of input samples used in training so far. Note that, maximum of this $\ell(x)$ value is often used in AL algorithms for sample selection [Yu and Kim, 2010, Wu et al., 2019]. Now, we now can substitute Equation 10 in Equation 9 to obtain the expression for $U_{model}(x)$ as

$$U_{model}(x) = \sigma(x)\ell(x)LP(x) \quad (12)$$

To compute $U_{model}(x)$ numerically, we still need to estimate the learning progress (LP) associated with input x . However, it is not feasible to compute LP for individual input samples, as the input space is not finite. So, we make a locality assumption and assign the same LP value to the points that belong to the same local region. In this study, we use equally spaced n -boxes as the local regions and compute LP for each region. Last p average RMSE errors for each region r_i are kept ($E^t(r_i)$), and are used to make a linear fit against $t = 1, 2, \dots, p$ so that $E^t(r_i) \approx m_i t + c_i$. The average errors are calculated with $E^t(r_i) = \frac{1}{|r_i|} \sum_{x \in r_i} e(x)$, where x indicates an executed input, i.e., a combination of (state, action) that falls within the region defining the range r_i , and $e(x)$ indicates the prediction error on x . The negative of the slope of the fit, $-m_i$ is technically the learning progress used in the literature [Kaplan and Oudeyer, 2004, Oudeyer et al., 2007], but here we map it to $[10^{-4}, 1]$ and enforce it to be positive to avoid singularity in Equation 10 with

$$LP(x) = LP(r_i) = \begin{cases} \frac{-2 \arctan m_i}{\pi}, & \text{if } m_i \leq 0 \\ 10^{-4}, & \text{otherwise} \end{cases} \quad (13)$$

So, now we have all the machinery necessary to compute an estimate of the uncertainty of the model associated with any potential input. In the next section, we explain how we make use of this to setup an active learning algorithm that a robot can use to explore its environment.

3.5 Sample Selection Based on Model Uncertainty

In this section, we describe the details of how our model, MUSEL, selects samples based on the computational elements discussed in the previous sections. The general flow and logic of MUSEL are illustrated in Figure 1. As we aim to optimize the data-gathering process of a robot in action-effect prediction tasks, we are typically faced with continuous input spaces. Thus, we adopt a population-based active learning approach.

The learning starts by initializing a bootstrapping input data set which is executed by the robot to create an initial observation set (see the Algorithm 1). To be concrete, first, m_{iter} number of i.i.d random state-action parameters, or simply inputs, are generated to create an initial set (\mathbb{X}_O) for robot to execute. Then, the robot executes the actions with parameters and environment states encoded by the inputs, and records the resulting effects as \mathbb{Y}_O (Algorithm 1, line 2).

Algorithm 1 Active Learning with MUSEL

Input environment $Env, n_{iter}, m_{init}, m_{cand}, k$
Output model M , data set \mathbb{D}_O

- 1: $\mathbb{X}_O \leftarrow \text{CREATESET}(m_{init})$ ▷ Initialize the training data set
- 2: $\mathbb{Y}_O \leftarrow \text{ROBOT:EXECUTEANDOBSERVE}(\mathbb{X}_O)$
- 3: $M \leftarrow \text{MODEL:INITIALIZE}()$
- 4: $i \leftarrow 0$
- 5: **while** $i < n_{iter}$ **do**
- 6: $M \leftarrow \text{MODEL:TRAIN}(\mathbb{X}_O, \mathbb{Y}_O)$
- 7: $\hat{\mathbb{Y}}_O \leftarrow \text{MODEL:GETPREDICTIONS}(\mathbb{X}_O)$
- 8: $\mathbb{X}_C \leftarrow \text{SAMPLE INPUT SPACE}(m_{cand})$ ▷ (Re)create the candidate inputs
- 9: $U_C \leftarrow \text{MODEL:ESTIMATESTDS}(\mathbb{X}_C)$ ▷ Estimate standard deviations
- 10: $LP \leftarrow \text{COMPUTE LP}(\mathbb{X}_O, \mathbb{Y}_O, \hat{\mathbb{Y}}_O)$
- 11: $\ell \leftarrow \text{COMPUTEDIST}(\mathbb{X}_O, \mathbb{X}_C)$
- 12: $U_{model} \leftarrow \text{ESTIMATE MODEL UNCERTAINTY}(\mathbb{X}_C, U_C, LP, \ell)$ ▷ Quantify model uncertainty
- 13: $X_C^* \leftarrow \text{SELECT TOPK}(\mathbb{X}_C, U_{model})$ ▷ Select top k state-action pairs
- 14: $Y_C^* \leftarrow \text{ROBOT:EXECUTEANDOBSERVE}(X_C^*)$ ▷ Observe effects of the selected inputs
- 15: $\mathbb{X}_O \leftarrow \text{UNION}(\mathbb{X}_O, X_C^*)$ ▷ Add the selected samples to the training data set
- 16: $\mathbb{Y}_O \leftarrow \text{UNION}(\mathbb{Y}_O, Y_C^*)$
- 17: $i \leftarrow i + 1$
- 18: **end while**
- 19: **return** M, \mathbb{D}_O

After this point, a model capable of learning input-output relations with uncertainty estimates, in this case SVGP, is trained with the bootstrapping data set, and the AL loop starts. At each iteration, the model is trained with the observed samples, and the predictions for the observed effects ($\hat{\mathbb{Y}}_O$) are saved (Algorithm 1, lines 6-7). Then \mathbb{X}_C is populated by random i.i.d. m_{cand} samples from the input space. This process is repeat at each iteration to have a Monte Carlo estimation of the input distribution. Subsequently, the model uncertainty values (U_{model}) are estimated by using standard deviation generated by the model, and LP and MD values are calculated as described in Section 3.4 (Algorithm 1, lines 9-12). After estimating the uncertainty values of the model, the candidate samples are sorted according to U_{model} in decreasing order, and the top k are selected for robot execution to generate new observation data (X_C^*), to be incorporated in training data for improving model prediction performance (Algorithm 1, line 13). After the robot executes the actions dictated by the formed set X_C^* , the observed effects are collected, and the corresponding input-effect pairs are added to the training data set (Algorithm 1, lines 15-16). The model is then trained with the updated dataset and subsequently, the steps for model uncertainty quantification is carried out. This sampling and learning loop continues until n_{iter} , a task dependent meta-parameter, iterations are completed.

4 Experiments and Results

To assess the feasibility and effectiveness of the MUSEL method, we designed a robotic tabletop setup where a manipulator robot is tasked with learning the effects of its actions. The environment includes either one or two spheres, where the robot can interact with one of them by hitting it at an arbitrary angle. We first present the one-sphere interaction scenario and compare the uncertainty quantification capabilities of the SVGP model to those of the standard GP model to ensure the reliability of the SVGP’s uncertainty estimates. We also visualize the dynamics of LP values observed during the learning process of MUSEL, as it is a novel component introduced for model uncertainty estimation.

After these sanity check experiments, in the single-sphere interaction task, we evaluate the sample efficiency of MUSEL by comparing it with random selection criteria. Additionally, we present the individual contributions of MUSEL components to the model uncertainty estimation. This is followed by ablation experiments, where we systematically isolate and verify the contributions of these components to the overall performance. Finally, we transition to the more complex two-sphere interaction task and evaluate the sample efficiency of our approach in this scenario. All experiments are performed in a dynamics simulation environment, PyBullet (version 3.2.6) [Coumans and Bai, 2016–2022].

4.1 One-Sphere Interaction Experiments

The environment for the learning experiments is designed as a confined table within the robot’s reach, where objects can bounce off the boundary walls according to the simulation physics. To break the symmetry in the task space, we introduced a diagonal wall placed across two consecutive walls of the table (see Figure 2). The robot is equipped with a single action, $push(\alpha)$, where $\alpha \in [-\pi/3, \pi/3] \subset \mathbb{R}$. The robot can accurately detect the position of the object as $\{pos_x, pos_y\}$ both before and after the action execution.

For implementing the push action, the robot’s end effector first moves to p_{start} and then hits the object by moving to p_{end} , where

$$\begin{aligned} p_{start} &= (pos_x - r \cos \alpha, pos_y - r \sin \alpha) \\ p_{end} &= (pos_x + r \cos \alpha, pos_y + r \sin \alpha) \end{aligned} \quad (14)$$

After the action is performed, the system waits for the sphere to stop, and the new position of the sphere is obtained by subtracting the initial position from it, giving the effect of the action as $y = \{\delta_x, \delta_y\}$. This experience is stored as an input-output pair $\{x, y\}$ and added to the training data (Algorithm 1, lines 15–16), where x defines the robot action and the initial state as $x = \{\sin \alpha, \cos \alpha, pos_x, pos_y\}$. Note that, as a common practice, α is encoded as $(\sin \alpha, \cos \alpha)$ to maintain input locality over the range of α .

For implementing MUSEL, we defined the meta-parameters of the method as follows: the number of active selection iterations, $n_{iter} = 3000$; the size of the initial training dataset, $m_{init} = 1$; and, finally, for the candidate inputs, $m_{cand} = 500$ and $k = 1$, representing the number of generated and selected inputs, respectively.

At each iteration, the selected learning engine (SVGP) is incrementally trained with the newly updated dataset. For SVGP training, we adopt a prioritized training scheme, selecting the $m_{train} = 2000$ least-trained samples for one epoch based on their training iteration count.

With this algorithm setting, the methods being compared are tested using 10 different random seeds to account for random effects. The methods are evaluated on a test dataset generated by sampling over a $25 \times 20 \times 20$ evenly distributed grid, where the grid counts correspond to the push angle and the x and y positions of the sphere, respectively.

4.1.1 Uncertainty Quantification

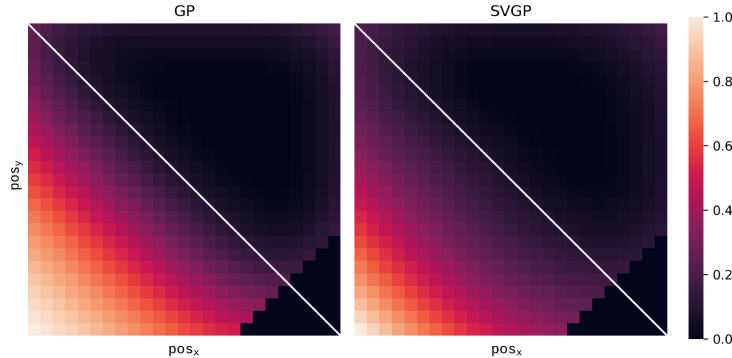


Figure 3: To compare the uncertainty quantification of GP and SVGP models, they are trained with data sampled from the upper diagonal triangle of the table. Then the models are queried for each angle at each grid. The grid-mean of the returned standard deviations are then used to create a normalized color map over the grid. Lighter colors indicate higher standard deviation/high uncertainty. The bottom right dark triangle is the region where a sphere cannot be placed (see Figure 2) thus not relevant for uncertainty estimation. This comparison shows that SVGP based uncertainty estimate is consistent with that of GP’s.

Before comparing the sample selection methods and analyzing their effects on learning, we evaluate the uncertainty quantification capability of the SVGP model against that of a typical GP model, as SVGP is used as the learning engine of MUSEL in the experiments reported in this paper. To ensure agnostic sampling, input samples are generated over a regular grid of $20 \times 25 \times 25$, spanning the full range of the (α, pos_x, pos_y) input space. The data from the upper right triangle of the table surface is then used as the training data, leaving the other half as unknown test points, which must be identified by the models' uncertainty estimates. After training for 2000 epochs, the uncertainty estimates, shown in Figure 3, are obtained, with the angle component averaged out. Although the models exhibit some differences in uncertainty values, their overall behavior is similar: uncertainty values increase in both models as the distance from the known training data increases. These findings demonstrate that SVGP can effectively capture the relative uncertainty associated with the input space, supporting its suitability as the learning engine for the MUSEL framework.

4.1.2 LP Values

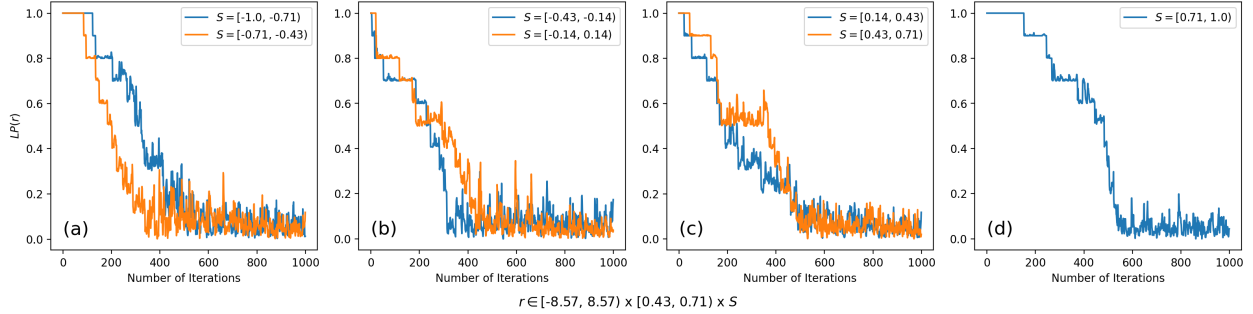


Figure 4: Typical LP profiles of illustrative regions defined with $\alpha, pos_x, pos_y \in [-8.57, 8.57] \times [-0.43, 0.71] \times S$ are shown, where S is indicated in the legend of each LP curve. For ease of comparison some LP curves are superimposed.

In MUSEL, inverse of LP is used as a proxy for data uncertainty (Section 3.4). However, unlike the standard deviation and minimum-distance (MD) metrics, which are computed per sample basis, LP is defined over predefined input regions, which may contain different numbers of samples during the processing of MUSEL. For the sphere interaction tasks, a 7×7 grid is used to define the LP regions in the $\alpha \times pos_x \times pos_y$ input space. The LP values computed for each region using Equation 13 are then assigned to the samples within the region to indicate the uncertainty associated with them. To show how LP values typically evolve in the LP regions, example LP profiles recorded during the learning of the one-sphere interaction task using the LP-only sample selection strategy are shown in Figure 4. Here, it can be seen that for LP regions near the boundaries (blue curves in (a) and (d), and orange curve in (c)) of the input domain remain elevated for a longer period compared to the regions away from the boundaries. This pattern suggests that learning in near-boundary regions continues to progress over an extended period. As such, sustained high LP values suggest that LP can serve as an effective indicator of model uncertainty, where errors can be reduced through further training.

On the other hand, the observed general trend in LP values indicates that they converge towards zero after approximately 500 iterations, which coincides with a reduction in test RMSE decrease rate (5a). This behavior aligns with the assumption that lower LP values indicate a lesser likelihood of reducible error. Note, however, that in some cases, an LP value may increase slightly after approaching zero due to the heterogeneity of samples belonging to a region. This suggests that, although LP is generally useful for capturing data uncertainty, it needs to be augmented for a more accurate estimation of data uncertainty, as discussed in Section 3.4.

4.1.3 Sample Efficiency in One-sphere Interaction Task

To assess the efficacy of MUSEL for robot self-learning, first, a simple one-sphere interaction task is considered, where the robot is required to learn the effect of its actions while interacting with a sphere. Two experiments are conducted: one with MUSEL and the other with pure random sample selection, both using SVGP as their learning engine. The experiments are repeated 10 times. We record the root mean squared error (RMSE) during the online learning process over a test set (see Section 4.1 for the details). Additionally, we record and visualize the sampling patterns of the two approaches to gain insights on the different performances exhibited by them. Figure 5a illustrates the sampling efficiency of MUSEL compared to random sampling, as evidenced by MUSEL's ability to reduce RMSE at a much steeper rate.

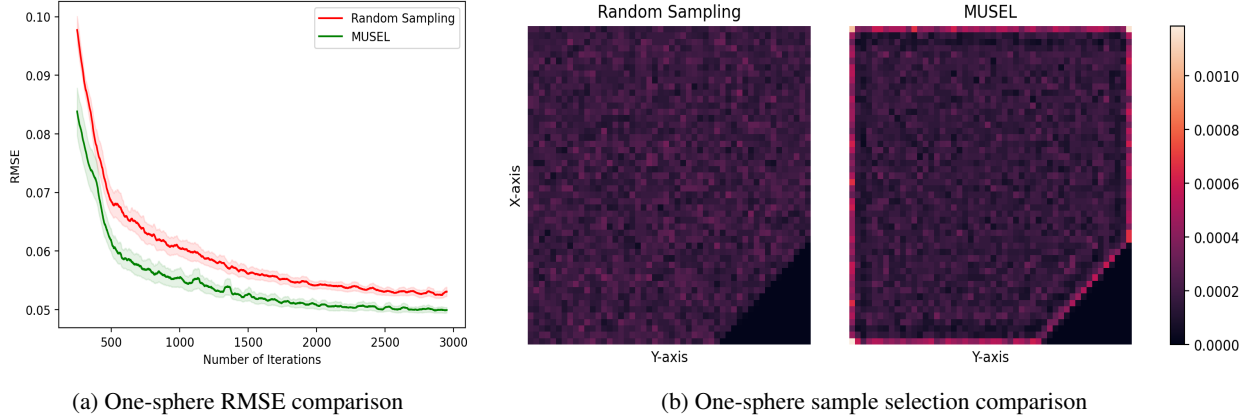


Figure 5: (a) MUSEL versus random sampling on the one-sphere experiment, given as RMSE vs. sampling iteration plot (with moving average smoothing with window size of 50). The curves represent the means over 10 repetitions, while the shaded areas indicate the standard error of the mean (SEM). (b) Histogram of sample selection by random sampling (left) and MUSEL (right) over the space of pos_x, pos_y with a grid of 50×50 over 10 repetitions (the histograms are normalized and scaled logarithmically for better visibility).

To understand the underlying reasons for the observed learning performances, observing the spatial distribution of the selected samples over the training period is instrumental. In Figure 5b, we present the sampling histogram of the two methods over the $\{pos_x, pos_y\}$ space. It can be seen that random sampling, as expected, generates a uniform distribution, while MUSEL exhibits a targeted selection pattern, emphasizing boundary regions. This is logical, as the behavior of the sphere near the boundaries is physically more complex than when it is in a central area. Thus, learning the action-effect patterns near the boundaries may require a larger number of interaction samples. MUSEL effectively detects this and consequently concentrates on these critical regions, leading to more efficient learning. In contrast, random sampling fails to learn these regions, resulting in slower overall learning and lower final prediction accuracy.

4.1.4 Individual Contributions of MUSEL Components

In this section, we investigate the contribution of individual components of MUSEL sample selection mechanism. This is done by using each component, namely the σ of learning engine (SVGP), learning progress (LP), and minimum-distance (MD) as the sole selection criterion for sample selection.

To be concrete, the learning performances of individual components of MUSEL, acting in isolation, are compared with MUSEL and the random selection strategy using RMSE values across learning iterations, as shown in Figure 6a. Using only the σ of the learning engine performs worse than all other approaches, likely due to the presence of high-uncertainty regions containing irreducible noise, i.e., data uncertainty. LP performs only slightly better than random selection due to its region-level granularity, which prevents it from reasoning about individual samples, causing it to fall back to random selection within a region. Interestingly, MD-based sample selection, known as Greedy Sampling on the Inputs (GSx) in the literature [Yu and Kim, 2010, Wu et al., 2019], performs almost as well as MUSEL.

To more effectively distinguish sample efficiency based on the number of samples, the RMSE values for each type of sampling are contrasted at iteration slices of 750, 1500, 2250, and 3000, as shown in the bar plots in Figure 6b. Paralleling the trend in the RMSE curves, MUSEL and MD-based strategy outperform other sampling schemes, with lower mean RMSE values favoring MUSEL in the early iterations. It is worth noting that only sampling with MD reaches a level comparable to MUSEL towards the end of the training.

As with the random and MUSEL-based sampling histograms shown in Figure 5a, we compute histograms for the methods based on σ , LP, and MD measures (see Figure 7). The learning engine-based uncertainty measure σ captures the overall uncertainty in the input space; however, its inability to distinguish between model and data uncertainties results in oversampling in regions with high data uncertainty, preventing overall reduction of errors over the input space. In LP-based sampling, we observe a similar focus diluted among the ranges of the boundary regions, as LP can only be computed at the regional level, and state-action pairs from the best region must be selected randomly. Section 4.1.2 shows LP values, which can be used to estimate model uncertainty, remain elevated in these areas for longer time, suggesting the model uncertainty values are also high in the boundary regions. Since the focus here is actually the reducible uncertainty, different than σ -based selection, LP-based approach samples from the central regions as well. Additionally, regions of the LP are equidistant, but the diagonal wall on the bottom-right reduces the LP space

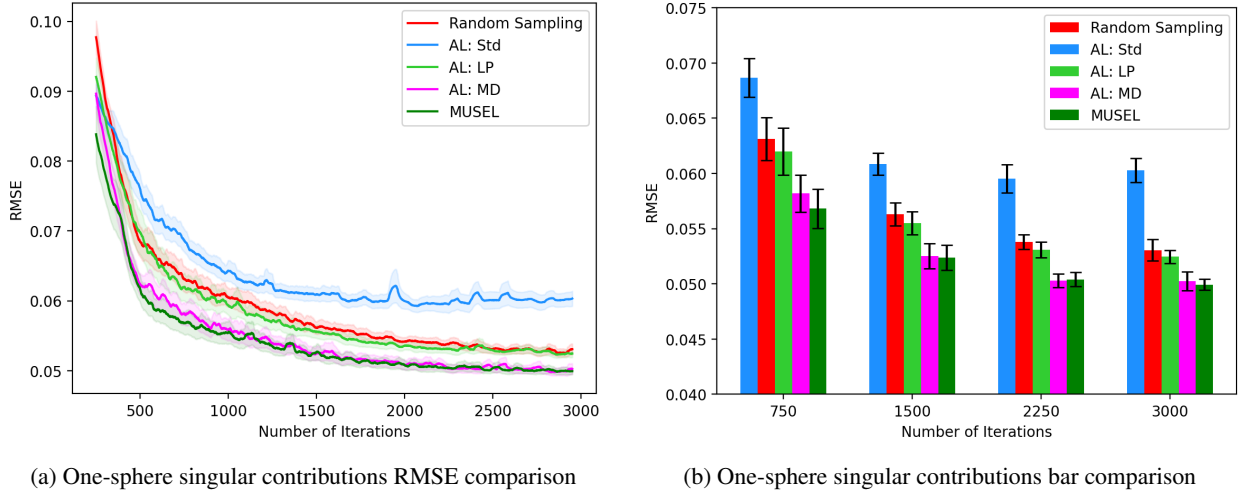


Figure 6: Comparison of single-measure-based sampling with MUSEL and random sampling across 10 repeated learning experiments based on test set RMSE. Variability in the measurements are computed as the standard error of the mean (SEM). (a) RMSE values for random selection (red), MUSEL (green), sampling based on standard deviation (blue), learning progress (magenta), and minimum-distance (light blue). (b) RMSE comparison at distinct iteration slices of 750, 1500, 2250, and 3000.

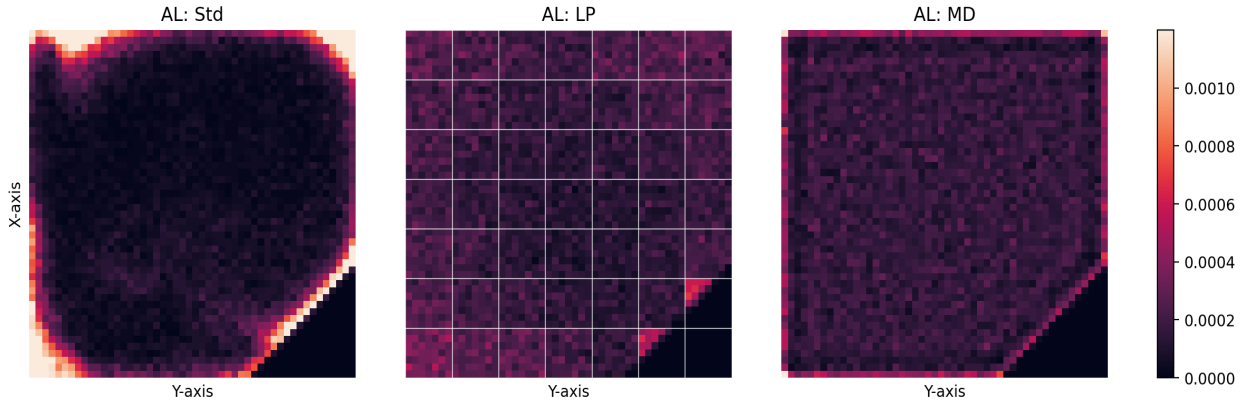


Figure 7: Histogram of the state-action pairs selected by the sampling strategies using standard deviation, σ (left), LP (middle), and MD (right). Test settings, including grid resolution, iteration count, and visualization parameters, are the same as in Figure 5b.

in two grid regions, resulting in a higher sampling density in those areas compared to all other regions, which are sampled approximately equally. The MD-based strategy operates without any knowledge of how the learning engine (SVGP in these experiments) performs; however, it prioritizes sampling near the boundaries of the input space due to their influence on the distribution of nearest training inputs. Coincidentally, these regions exhibit higher model uncertainty due to the robotic task adopted. Therefore, the MD algorithm demonstrates strong performance compared to other single-measure sampling strategies. It is also worth noting that, unlike σ , it avoids excessive focusing on data-uncertainty-bound areas; and, in contrast to LP, it is capable of differentiating individual samples rather than distributing the same value to all samples in a given region.

While MUSEL and the MD-based strategy select samples from similar regions, our results (see Figure 6) show that MUSEL achieves better mean sample efficiency in the earlier iterations. This improvement can be attributed to MUSEL’s approach of integrating information from multiple sources, namely, the total uncertainty estimate from the learning engine (σ), how learning progresses (LPs) and how well the selected samples are distributed (MD).

4.1.5 Ablation Study

To assess the necessity and importance of MUSEL’s components for its operation, we conducted a set of ablation experiments using the same evaluation procedure as in the previous section. These ablation experiments also allow us to observe how the combinations of σ , LP, and MD synergistically work together to select the most informative samples for faster learning.

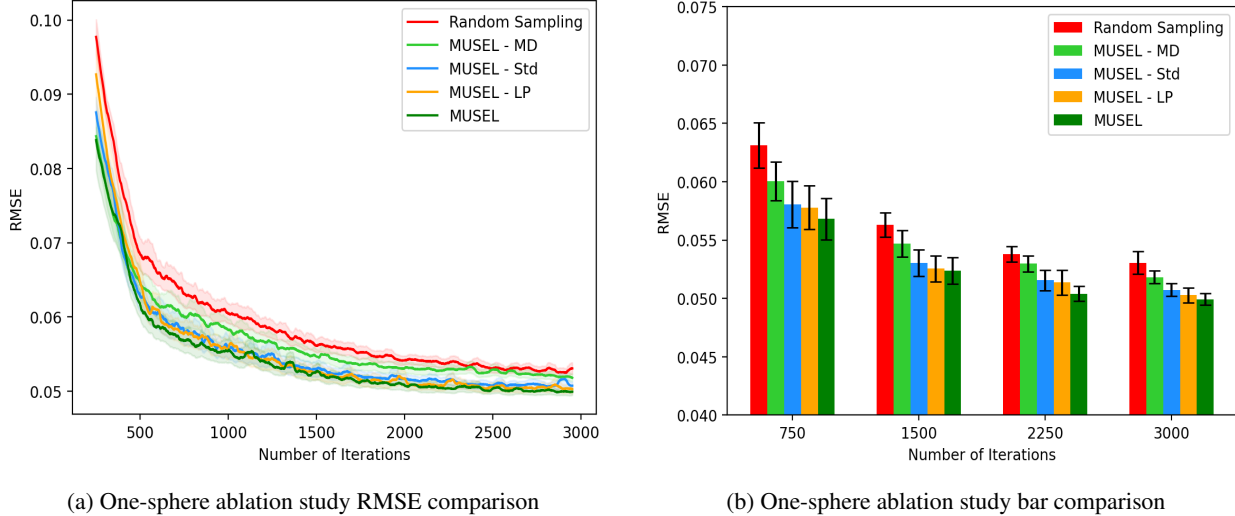


Figure 8: Comparison of ablated methods with MUSEL and random sampling (plotting conventions are the same as in Figure 6). (a) Test set RMSE errors are shown for random sampling (red), MUSEL (green), and ablations of MD (light green), Std (σ) (light blue) and LP (orange). (b) Comparison of RMSE across distinct iterations 750, 1500, 2250, and 3000.

The RMSE results for the ablated versions of MUSEL, shown in Figure 8a, reveal that in the one-sphere task, the most significant performance degradation occurs when the MD component is removed. This is unsurprising, as MD exhibited the best solo performance, as detailed in Section 4.1.4. In contrast, removing the LP component results in the smallest performance reduction, likely due to its regional selection strategy. Similarly, ablating the Std (σ) component causes a comparable decline in performance, possibly because the other criteria can still capture model uncertainty without explicitly incorporating σ , as shown in Section 4.1.4.

Another way of looking at the ablation results is to interpret them as outcomes from pairs of measures. The σ + LP pair (MUSEL - MD) improves performance compared to the individual use of components, indicating that LP helps eliminate some of the data uncertainty captured by standard deviation (σ), but this pair still remains less effective than other combinations. The σ + MD combination (MUSEL - LP) also performs better than standard deviation σ alone, achieving the best performance among the ablation pairs. On the other hand, surprisingly, this is not true for MD. Although MD is expected to reduce the stubborn focus of σ on irreducible error regions while exploiting its uncertainty information, it appears that this does not happen, and σ acts as a hindrance to MD. The LP + MD (MUSEL - σ) pair performs slightly better than LP, likely because it enables instance-wise prioritization rather than region-wise selection. However, it performs worse than MD, likely due to competing priorities, with LP focusing on error trends and MD on spatial diversity.

To provide snapshots of model performance at different stages, the RMSE values for random sampling, MUSEL, and ablation study candidates at the 750th, 1500th, 2250th, and 3000th iterations are compared in Figure 8b. Among the ablation study candidates, the ablation of LP demonstrates the lowest mean RMSE values; however, it fails to outperform MD-based selection in Section 4.1.4. MUSEL has the best mean error across all iterations, with the difference decreasing over time as iterations progress.

The histograms of sample selections for the three ablated versions of MUSEL are shown in Figure 9. The observed selection patterns align with the sample efficiency comparisons presented in Figure 8. Selecting samples based on standard deviation alone prioritizes areas with high data uncertainty; however, pairing it with either LP or MD appears to balance this focus. The combination of standard deviation with MD (i.e., LP ablation) results in a selection pattern that closely resembles MUSEL’s selections, which demonstrates the best performance among the pairs. However, this combination does not fully account for the data uncertainty inherent in the estimations and places greater emphasis

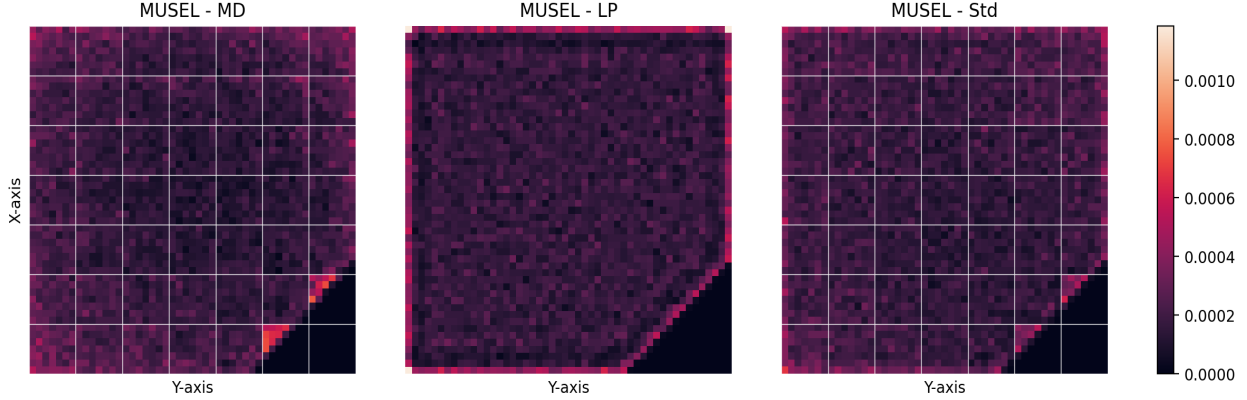


Figure 9: Histograms of selected state-action pairs with MD-ablated (left), LP-ablated (middle), and σ -ablated (right) versions of MUSEL are shown (the grid resolution, iteration count, and visualization parameters are the same as Figure 5b).

on boundary points. As stated in the performance evaluation, pairing MD with LP partially reduces MD’s focus on boundary points, resulting in a learning performance that lies between the individual performances of MD and LP.

4.2 Two-Sphere Interaction Experiments

4.2.1 General Overview

In the two-sphere interaction experiments (see Figure 10), the robot is again equipped with a push action similar to that in Section 4.1, which is always directed at a predetermined ‘cue’ sphere. The other sphere is placed at a fixed location, influencing the environment dynamics by being hit by the cue sphere. Thus, the input space of the task remains the same as in the one-sphere interaction task, but the action-effect dynamics become more complex. The motivation behind designing this setup is to examine the impact of a controlled increase in task complexity.

While the input and output dimensions remain the same as in the one-sphere interaction task, we ensure that the cue sphere cannot be placed in a position that would make it intersect with the other sphere, as this would result in a collision and subsequent motion due to the physics simulator used. Thus, the valid initial input configuration space becomes asymmetric and more complex, further adding to the learning difficulty.

For implementing MUSEL in the two-sphere interaction task, we used the same meta-parameters as in the one-sphere setup: $n_{iter} = 3000$, $m_{init} = 1$, $m_{cand} = 500$, and $k = 1$. Similarly, the SVGP learning engine was incrementally trained with the updated dataset using a prioritized training scheme, selecting the $m_{train} = 2000$ least-trained samples for one epoch based on their training iteration count. The test dataset was generated on a $20 \times 25 \times 25$ grid, corresponding to the push angle, α , and the table locations, pos_x and pos_y , respectively.

4.2.2 Learning Efficiency Comparison

In the experiments presented in this section, we compare MUSEL to random sampling and MD-based sampling, the latter being the strongest competitor to MUSEL, according to the one-sphere task experiments.

The performance of the models is presented in Figure 11 using the conventions established in the one-sphere interaction task. The results show that MUSEL and MD-based sampling achieve higher sample efficiency compared to random sampling, paralleling the findings from the one-sphere experiments. An interesting observation is that the improvement over random selection is even more pronounced in the two-sphere interaction task (see Figure 5). This suggests that

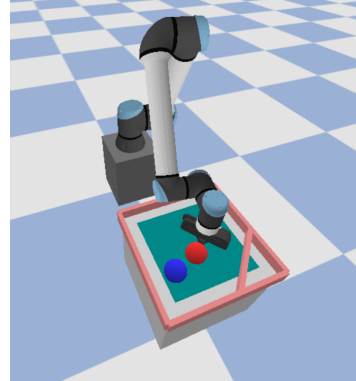


Figure 10: Two-sphere interaction task: the red sphere is the cue sphere that the robot can interact with. The blue sphere moves according to physics but is reset to a predetermined, fixed position before each robot action.

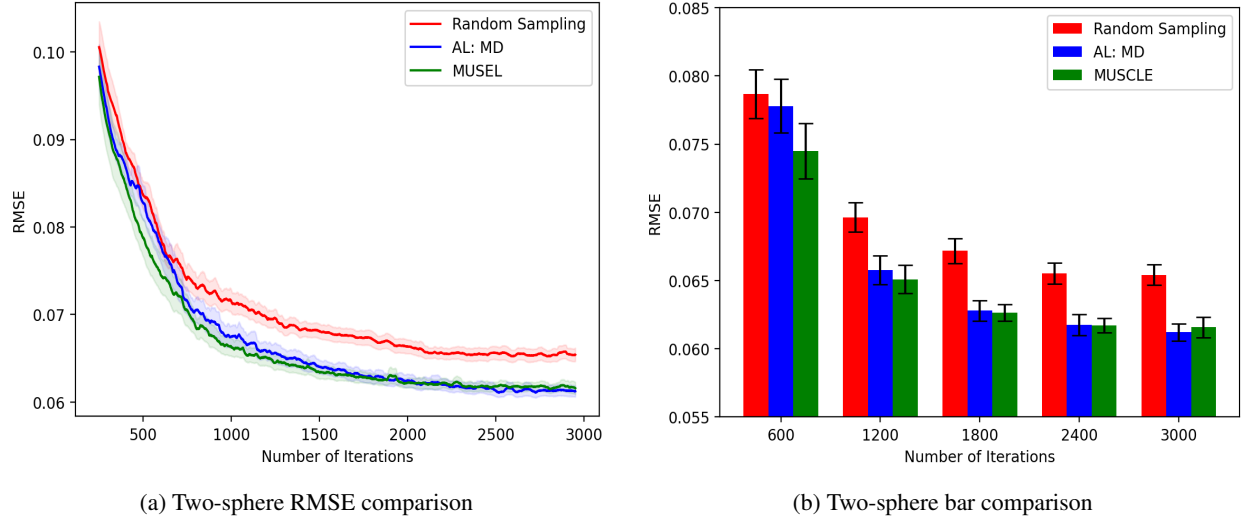


Figure 11: RMSE curves of MUSEL (green), MD-based sampling (blue), and random sampling (red) are given as a function of the sampling iteration during learning in the two-sphere interaction task (a), along with the bar plot comparisons at specific iterations (b). The plotting conventions are the same as in Figure 6.

more complex learning tasks may benefit more from guided sample selection. Another notable point is the increased performance gap between MUSEL and MD-based sampling during the first half of learning, compared to the one-sphere interaction task.

In addition, to assess the differential ability of models to perform well in low-sampling regimes, we also analyze the learning performance at the 600th, 1200th, 1800th, 2400th, and 3000th iteration slices (Figure 11b). Random sampling clearly performs the worst among the methods. MD-based sampling outperforms random selection and continues to be a competitive method, as observed in the one-sphere task (see Section 4.1.4). MUSEL demonstrates the best initial performance and consistently achieves the lowest RMSE throughout the learning process, except at the 3000th iteration.

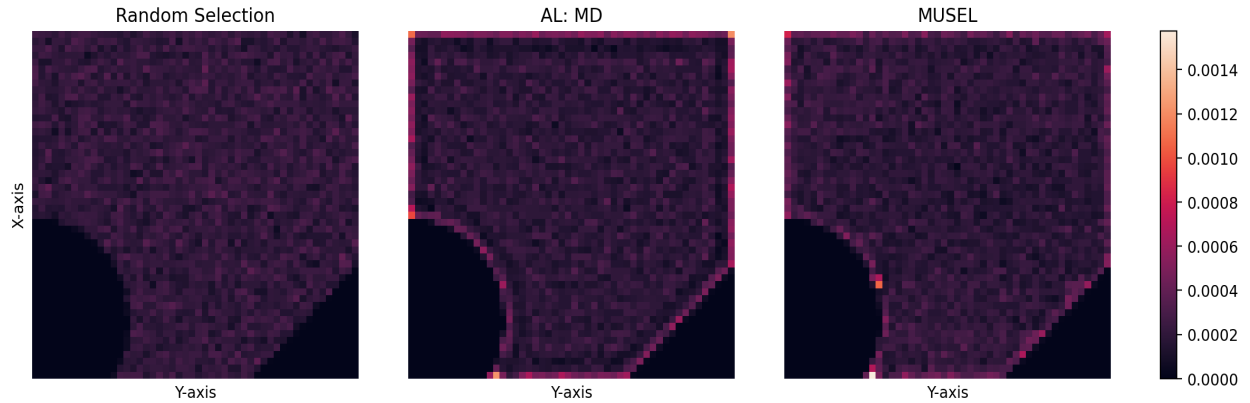


Figure 12: Selected state-action pairs using random sampling (left), MD (middle), and MUSEL (right). The radial empty space in the bottom-left is due to the second sphere, where the cue sphere cannot be located and is therefore irrelevant for sampling. The plotting conventions are the same as in Figure 5a.

To see how the sampling strategies influence the coverage of the input space and their potential impact on model performance, the selected samples of each method is illustrated in Figure 12. In random selection case, as in the one-sphere interaction task, samples are distributed more evenly across the sample space. The MD-based sampling follows a similar pattern, except that sample accumulation occurs near the input boundaries. MUSEL sampling appears similar to MD-based sampling; however, slight differences can be detected: boundary accumulation is less pronounced,

and more intense sampling, compared to MD, is observed in certain specific regions. These differences may contribute to MUSEL’s superior performance, particularly during the early iterations.

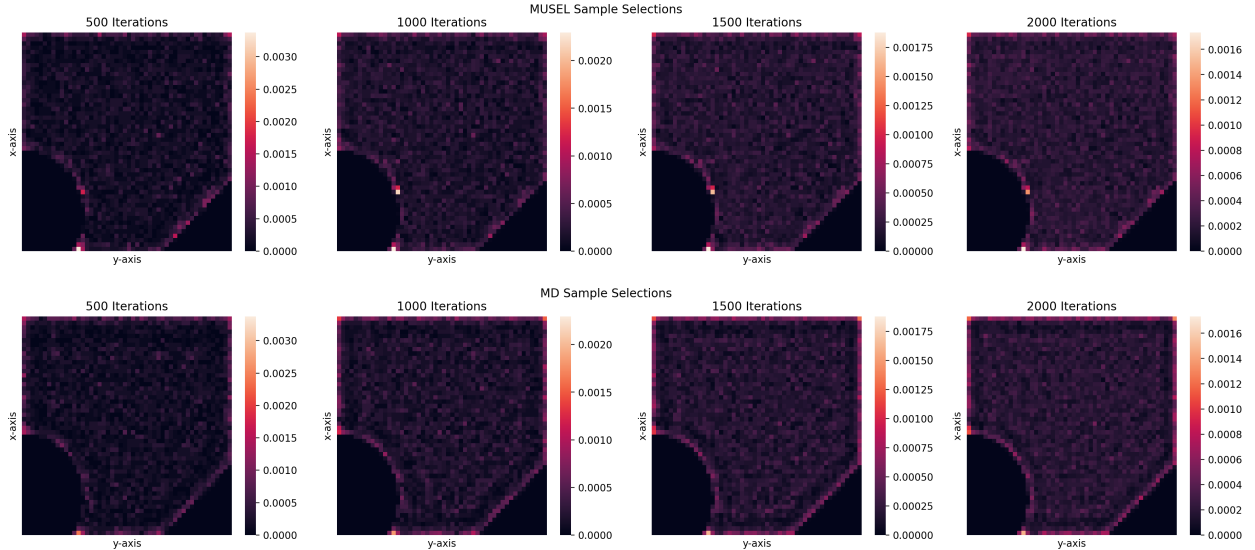


Figure 13: Sample distributions obtained by MUSEL (upper panels) and MD-based sampling (lower panels) given at distinct iterations. The plotting conventions are the same as those in Figure 5a.

From the RMSE curves of MUSEL and MD-based sampling (see Figure 11), it is evident that MUSEL makes better sample selections from the beginning. To analyze the sample distributions contributing to this improved performance, we computed the sampling histograms of both models at the 500th, 1000th, 1500th, and 2000th iterations (Figure 13). The sampling distributions indicate that MD-based strategy start to accumulate samples evenly from input boundary quickly, and this trend continues until the end of learning. MUSEL, while also having a bias toward the boundary, initially samples from the fixed sphere boundary and the diagonal wall, resulting in intensified sampling in a few specific regions. Then it balances overall performance by selecting more samples from the central regions compared to MD. To quantify the observations above, we counted the number of boundary samples generated by both models, averaging the results over 10 tests, as presented in Table 1.

Method	500 Iterations	1000 Iterations	1500 Iterations	2000 Iterations
MUSEL	95.8	158.4	225.0	287.6
MD	113.7	211.0	299.2	384.0

Table 1: Counts for two methods across 4 iterations.

The results confirm the intuition that a sampling approach detached from the ongoing learning performance, such as MD, is less suitable for complex learning tasks where regions of importance must be discovered by the sampling strategy to guide learning. The proposed model, MUSEL, offers a promising solution in this direction.

5 Conclusion

In this study, we introduced MUSEL (Model Uncertainty for Sample-Efficient Learning), a novel sample-efficient active learning framework for robot self-supervised learning. The effectiveness of MUSEL is demonstrated in simulated robotic experiments through ablation studies and comparisons with several baselines. Unlike previous approaches, MUSEL integrates model uncertainty directly into its sample selection strategy by extracting it from the total uncertainty estimate provided by a Stochastic Variational Gaussian Process (SVGP). This is achieved through the novel use of Learning Progress (LP) and minimum-distance (MD) metrics, enabling MUSEL to adaptively choose the most informative actions and address the high costs associated with extensive data collection in robot learning.

The findings presented in this paper have valuable implications for improving sample-efficient robot learning. MUSEL presents a data-efficient training framework, making it particularly suitable for real-world scenarios where data collection

is expensive or time-consuming. Furthermore, the use of SVGP as the learning engine enhances scalability, enabling it to handle larger datasets more efficiently compared to traditional Gaussian Processes. Its ability to perform active learning on continuous input spaces through Monte Carlo sampling broadens its applicability to other robotic tasks, contributing to the development of more intelligent and adaptable robotic systems.

Despite these promising results, there is room for improvement. MUSEL’s sample selection logic can result in high computation times for high-dimensional problems, posing challenges for real-time applications requiring high-speed, online sampling. Additionally, the MD component adopted in MUSEL tends to favor input samples near the boundaries of the input space. While this bias provides an advantage in the current tasks due to higher model uncertainty in boundary regions, it may hinder performance in tasks where uncertainty is higher in non-boundary areas. Therefore, future work should explore ways to reduce computation time, mitigate unintended sampling biases, and implement the system on real robotic hardware, enabling the robot to learn through unsupervised, continual self-learning without human intervention.

6 ACKNOWLEDGMENTS

This work was supported by the Japan Society for the Promotion of Science KAKENHI Grant Number JP23K24926, and by the project JPNP16007 commissioned by the New Energy and Industrial Technology Development Organization (NEDO).

References

- Alper Ahmetoglu, M Yunus Seker, Justus Piater, Erhan Oztop, and Emre Ugur. Deepsym: Deep symbol generation and rule learning for planning from unsupervised robot interaction. *Journal of Artificial Intelligence Research*, 75: 709–745, 2022.
- M Yunus Seker, Ahmet E Tekden, and Emre Ugur. Deep effect trajectory prediction in robot manipulation. *Robotics and Autonomous Systems*, 119:173–184, 2019.
- Emre Ugur, Erhan Oztop, and Erol Sahin. Goal emulation and planning in perceptual space using learned affordances. *Robotics and Autonomous Systems*, 59(7-8):580–595, 2011.
- David Ha and Jürgen Schmidhuber. World models. *arXiv preprint arXiv:1803.10122*, 2018.
- Adrien Baranes and Pierre-Yves Oudeyer. Active learning of inverse models with intrinsically motivated goal exploration in robots. *Robotics and Autonomous Systems*, 61(1):49–73, 2013.
- Kuo Li, Xinze Jin, Qing-Shan Jia, Dongchun Ren, and Huaxia Xia. An oeba-based method for efficient sample collection in reinforcement learning. *IEEE Transactions on Automation Science and Engineering*, 2023.
- Pierre-Yves Oudeyer, Frdric Kaplan, and Verena V Hafner. Intrinsic motivation systems for autonomous mental development. *IEEE transactions on evolutionary computation*, 11(2):265–286, 2007.
- Alexandre Péré, Sébastien Forestier, Olivier Sigaud, and Pierre-Yves Oudeyer. Unsupervised learning of goal spaces for intrinsically motivated goal exploration. *arXiv preprint arXiv:1803.00781*, 2018.
- Melisa Idil Sener, Yukie Nagai, Erhan Oztop, and Emre Ugur. Exploration with intrinsic motivation using object–action–outcome latent space. *IEEE Transactions on Cognitive and Developmental Systems*, 15(2):325–336, 2021.
- Serkan Bugur, Erhan Oztop, Yukie Nagai, and Emre Ugur. Effect regulated projection of robot’s action space for production and prediction of manipulation primitives through learning progress and predictability-based exploration. *IEEE Transactions on Cognitive and Developmental Systems*, 13(2):286–297, 2019.
- Burr Settles. Active learning literature survey. Computer Sciences Technical Report 1648, University of Wisconsin–Madison, 2009. URL <https://minds.wisconsin.edu/handle/1793/60660>.
- Tianxu He, Shukui Zhang, Jie Xin, Pengpeng Zhao, Jian Wu, Xuefeng Xian, Chunhua Li, and Zhiming Cui. An active learning approach with uncertainty, representativeness, and diversity. *The Scientific World Journal*, 2014(1):827586, 2014.
- Christoph Käding, Erik Rodner, Alexander Freytag, Oliver Mothes, Björn Barz, Joachim Denzler, and Carl Zeiss AG. Active learning for regression tasks with expected model output changes. In *BMVC*, page 103, 2018.
- Wenbin Cai, Ya Zhang, and Jun Zhou. Maximizing expected model change for active learning in regression. In *2013 IEEE 13th international conference on data mining*, pages 51–60. IEEE, 2013.
- Masashi Sugiyama and Shinichi Nakajima. Pool-based active learning in approximate linear regression. *Machine Learning*, 75:249–274, 2009.

- Dongrui Wu. Pool-based sequential active learning for regression. IEEE transactions on neural networks and learning systems, 30(5):1348–1359, 2018.
- Ziang Liu, Xue Jiang, Hanbin Luo, Weili Fang, Jiajing Liu, and Dongrui Wu. Pool-based unsupervised active learning for regression using iterative representativeness-diversity maximization (irdm). Pattern Recognition Letters, 142: 11–19, 2021.
- Dongrui Wu, Chin-Teng Lin, and Jian Huang. Active learning for regression using greedy sampling. Information Sciences, 474:90–105, 2019.
- Annalisa T Taylor, Thomas A Berrueta, and Todd D Murphey. Active learning in robotics: A review of control principles. Mechatronics, 77:102576, 2021.
- M. van Deursen. Population-based active learning for black-box regression. Master’s thesis, Delft University of Technology, Delft, Netherlands, October 2020. Available at <http://repository.tudelft.nl/>.
- James Hensman, Nicolo Fusi, and Neil D Lawrence. Gaussian processes for big data. arXiv preprint arXiv:1309.6835, 2013.
- Frédéric Kaplan and Pierre-Yves Oudeyer. Maximizing learning progress: an internal reward system for development. In Embodied Artificial Intelligence: International Seminar, Dagstuhl Castle, Germany, July 7-11, 2003. Revised Papers, pages 259–270. Springer, 2004.
- David A Cohn, Zoubin Ghahramani, and Michael I Jordan. Active learning with statistical models. Journal of artificial intelligence research, 4:129–145, 1996.
- Yifan Fu, Bin Li, Xingquan Zhu, and Chengqi Zhang. Active learning without knowing individual instance labels: a pairwise label homogeneity query approach. IEEE Transactions on Knowledge and Data Engineering, 26(4): 808–822, 2013.
- Iker Lluvia, Elena Lazkano, and Ander Ansuategi. Active mapping and robot exploration: A survey. Sensors, 21(7): 2445, 2021.
- Ian Abraham, Ahalya Prabhakar, Mitra JZ Hartmann, and Todd D Murphey. Ergodic exploration using binary sensing for nonparametric shape estimation. IEEE robotics and automation letters, 2(2):827–834, 2017.
- Olov Andersson, Mariusz Wzorek, and Patrick Doherty. Deep learning quadcopter control via risk-aware active learning. In Proceedings of the Thirty-First AAAI Conference on Artificial Intelligence, pages 3814–3820, 2017. doi:10.1609/aaai.v31i1.11041.
- Guilherme Maeda, Marco Ewerton, Takayuki Osa, Baptiste Busch, and Jan Peters. Active incremental learning of robot movement primitives. In Conference on Robot Learning, pages 37–46. PMLR, 2017.
- Sean Segal, Nishanth Kumar, Sergio Casas, Wenyan Zeng, Mengye Ren, Jingkan Wang, and Raquel Urtasun. Just label what you need: Fine-grained active selection for p&p through partially labeled scenes. In Conference on Robot Learning, pages 816–826. PMLR, 2022.
- Dohyun Jang, Jaehyun Yoo, Clark Youngdong Son, and H Jin Kim. Fully distributed informative planning for environmental learning with multi-robot systems. arXiv preprint arXiv:2112.14433, 2021.
- James Marshall, Doug Blank, and Lisa Meeden. An emergent framework for self-motivation in developmental robotics. In Proceedings of the International Conference on Development and Learning, 2004.
- Xiao Huang and John Weng. Novelty and reinforcement learning in the value system of developmental robots. In Proceedings of the 2nd International Workshop on Epigenetic Robotics, pages 47–55, 2002. Lund University Cognitive Studies, vol. 94.
- Rein Houthoofd, Xi Chen, Yan Duan, John Schulman, Filip De Turck, and Pieter Abbeel. Vime: Variational information maximizing exploration. Advances in neural information processing systems, 29, 2016.
- Joshua Achiam and Shankar Sastry. Surprise-based intrinsic motivation for deep reinforcement learning. arXiv preprint arXiv:1703.01732, 2017.
- Hanne Say and Erhan Oztop. A model for cognitively valid lifelong learning. In 2023 IEEE International Conference on Robotics and Biomimetics (ROBIO), pages 1–7. IEEE, 2023.
- Adrien Baranes and Pierre-Yves Oudeyer. R-iac: Robust intrinsically motivated exploration and active learning. IEEE Transactions on Autonomous Mental Development, 1(3):155–169, 2009.
- Scott Cheng-Hsin Yang, Daniel M Wolpert, and Máté Lengyel. Theoretical perspectives on active sensing. Current opinion in behavioral sciences, 11:100–108, 2016.
- Tipakorn Greigarn, Michael S Branicky, and M Cenk Çavuşoğlu. Task-oriented active sensing via action entropy minimization. IEEE Access, 7:135413–135426, 2019.

- Alexander Tschantz, Anil K Seth, and Christopher L Buckley. Learning action-oriented models through active inference. PLoS computational biology, 16(4):e1007805, 2020.
- Gang Chen, Dongxiao Sun, Wei Dong, Xinjun Sheng, Xiangyang Zhu, and Han Ding. Computationally efficient trajectory planning for high speed obstacle avoidance of a quadrotor with active sensing. IEEE Robotics and Automation Letters, 6(2):3365–3372, 2021.
- Olga Napolitano, Marco Cognetti, Lucia Pallottino, Dimitrios Kanoulas, Paolo Salaris, and Valerio Modugno. Active sensing for data quality improvement in model learning. IEEE Control Systems Letters, 2024.
- Yazhou Yang and Marco Loog. Active learning using uncertainty information. In 2016 23rd International Conference on Pattern Recognition (ICPR), pages 2646–2651. IEEE, 2016.
- Yi Yang, Zhigang Ma, Feiping Nie, Xiaojun Chang, and Alexander G Hauptmann. Multi-class active learning by uncertainty sampling with diversity maximization. International Journal of Computer Vision, 113:113–127, 2015.
- Jingbo Zhu, Huizhen Wang, Benjamin K Tsou, and Matthew Ma. Active learning with sampling by uncertainty and density for data annotations. IEEE Transactions on audio, speech, and language processing, 18(6):1323–1331, 2009.
- Jakob Gawlikowski, Cedrique Rovile Njietcheu Tassi, Mohsin Ali, Jongseok Lee, Matthias Humt, Jianxiang Feng, Anna Kruspe, Rudolph Triebel, Peter Jung, Ribana Roscher, et al. A survey of uncertainty in deep neural networks. arXiv preprint arXiv:2107.03342, 2021.
- Murat Sensoy, Lance Kaplan, and Melih Kandemir. Evidential deep learning to quantify classification uncertainty. Advances in neural information processing systems, 31, 2018.
- Philipp Oberdiek, Matthias Rottmann, and Hanno Gottschalk. Classification uncertainty of deep neural networks based on gradient information. In Artificial Neural Networks in Pattern Recognition: 8th IAPR TC3 Workshop, ANNPR 2018, Siena, Italy, September 19–21, 2018, Proceedings 8, pages 113–125. Springer, 2018.
- José G Dias and Jeroen K Vermunt. Bootstrap methods for measuring classification uncertainty in latent class analysis. In Compstat 2006-Proceedings in Computational Statistics: 17th Symposium Held in Rome, Italy, 2006, pages 31–41. Springer, 2006.
- José Mena, Oriol Pujol, and Jordi Vitrià. A survey on uncertainty estimation in deep learning classification systems from a bayesian perspective. ACM Computing Surveys (CSUR), 54(9):1–35, 2021.
- Rohit Tripathy, Ilias Bilonis, and Marcial Gonzalez. Gaussian processes with built-in dimensionality reduction: Applications to high-dimensional uncertainty propagation. Journal of Computational Physics, 321:191–223, 2016.
- Alexander Amini, Wilko Schwarting, Ava Soleimany, and Daniela Rus. Deep evidential regression. Advances in Neural Information Processing Systems, 33:14927–14937, 2020.
- Nis Meinert and Alexander Lavin. Multivariate deep evidential regression. arXiv preprint arXiv:2104.06135, 2021.
- Nis Meinert, Jakob Gawlikowski, and Alexander Lavin. The unreasonable effectiveness of deep evidential regression. Proceedings of the AAAI Conference on Artificial Intelligence, 37(8):9134–9142, Jun. 2023. doi:10.1609/aaai.v37i8.26096.
- Christopher Williams and Carl Rasmussen. Gaussian processes for regression. Advances in neural information processing systems, 8, 1995.
- Michalis Titsias. Variational learning of inducing variables in sparse gaussian processes. In Artificial intelligence and statistics, pages 567–574. PMLR, 2009.
- Yarin Gal, Mark Van Der Wilk, and Carl Edward Rasmussen. Distributed variational inference in sparse gaussian process regression and latent variable models. Advances in neural information processing systems, 27, 2014.
- David M Blei, Alp Kucukelbir, and Jon D McAuliffe. Variational inference: A review for statisticians. Journal of the American statistical Association, 112(518):859–877, 2017.
- Carl Edward Rasmussen and Christopher KI Williams. Gaussian Processes for Machine Learning. MIT Press, 2006.
- Heejin Lee, Seunghyun Lee, and Byung Cheol Song. Data and model uncertainty aware salient object detection. IEEE Access, 2024.
- Hwanjo Yu and Sungchul Kim. Passive sampling for regression. In 2010 IEEE international conference on data mining, pages 1151–1156. IEEE, 2010.
- Erwin Coumans and Yunfei Bai. Pybullet, a python module for physics simulation for games, robotics and machine learning. <http://pybullet.org>, 2016–2022.